Supplement of Atmos. Chem. Phys., 19, 1703–1719, 2019
https://doi.org/10.5194/acp-19-1703-2019-supplement

Atmospheric Chemistry and Physics
Open Access

Supplement of

Evidence for a major missing source in the global chloromethane budget from stable carbon isotopes

Enno Bahlmann et al.

Correspondence to: Enno Bahlmann (enno.bahlmann@leibniz-zmt.de)

Further experimental details, results and discussion

The smog chamber used for the CH_3Cl and CH_4 degradation experiments is depicted in figure S1 (taken from Keppler et al., 2018). It is made of Teflon FEP-film (fluorinated ethylene propylene, FEP 200A, DuPont, Wilmington, DE, USA). Prior to the experiments, the chamber was flushed with hydrocarbon-free zero air (zero-air-generator, cmc instruments, <1 nmol mol^{-1} of O_3, <0.5 nmol mol^{-1} NO_X, <0.1 nmol mol^{-1} of CH_4) at a flushing flow rate of 20 dm^3 min^{-1} and cleaned with OH radicals from the photolysis of O_3 for at least 8 h. In between the experiments, the chamber was typically cleaned for 6 to 8 h. During the experiments the flushing flow rate through the chamber was between 0.6 and 4 dm^3 min^{-1}. To warrant a zero air environment and avoid intrusion of ambient air, the chamber was operated with a slight overpressure of 0.5-1 Pa, logged with a differential pressure sensor (Kalinsky Elektronik DS1). A custom made Teflon-PTFE fan inside the chamber, placed directly below the zero air inlet, ensured constant mixing throughout the experiments. The experiments were carried out at a temperature of (20.5 ± 0.3) °C The ozone generation method and the monitoring of O_3, NO and NO_x are provided in the main manuscript. Initial CH_3Cl mixing ratios were between 1 and 10 µmol mol^{-1}. Perfluorohexane (PFH), (25 ± 5) µmol mol^{-1} initial mixing ratio), was used as an internal standard to correct the resulting concentrations for dilution. The mixing ratios of CH_3Cl and PFH were monitored by GC-MS (HP 6890 gas chromatograph coupled to a MSD 5973 mass spectrometer; Agilent Technologies, Palo Alto, CA) with a time resolution of 15 min throughout the experiments. Aliquouts of 5 ml were taken from the chamber with a gas-tight syringe, injected into a stream of helium (30 ml min^{-1}) and directed to a pre-concentration unit attached to the GC-MS. The pre-concentration unit consisted of a simple 8 port valve (Valco) equipped with two cryo-traps made of fused silica, which are immersed in liquid nitrogen for trapping the analytes. With each sample, a gaseous standard (5 ml of 100 µmol mol^{-1} CH_3Cl in N_2) was measured using the second cryo-trap. At the beginning of each experiment, the ratio of CH_3Cl and PFH, used to calculate the residual fraction of CH_3Cl, was typically monitored for 2 h. The reproducibility for the determination of the CH_3Cl to PFH ratio used to calculate residual fraction (f_t) of CH_3Cl was between 1.4 and 2.0 % (1σ).

Atomic chlorine (Cl) was generated via photolysis of molecular chlorine (Cl_2) at a relative humidity of less than 1% by a solar simulator with an actinic flux comparable to the sun in mid-summer in Germany. The solar simulator (Behnke et al., 1988)

consists of 7 medium pressure arc lamps (Osram HMI 1200 W) with aluminum coated reflectors. To obtain a spectrum comparable to atmospheric conditions, the light is filtered by a borosilicate glass filter (Schott, Tempax, 3 mm) for UV and by a ~2 cm water layer (connected to a heat exchanger) for infrared radiation. A previously published spectrum (Palm et al., 1998) has been updated (fig. S1, lower panel) after renewing the borosilicate filter (Bleicher et al., 2014). The Cl degradation experiments were carried out with intermittent time intervals of photolysis and sampling. Typically, Cl_2 was added to obtain a mixing ratio in the chamber between 2 and 10 µmol mol^{-1} and was photolyzed for 10 - 30 min before the samples for the carbon isotope determination were taken.

In our study, OH was generated via the photolysis of ozone at 253.7 nm in the presence of water vapour at a relative humidity of 70 ±5 %). This is a well-established, efficient method for OH radical generation (Cantrell et al. 1990, DeMore 1992). In the CH_3Cl + OH experiments, an initial level of 2000 µmol mol^{-1} of H_2 was added for scavenging chlorine radicals originating from the photolysis or oxidation of formyl chloride (HCOCl) formed as an intermediate in the reaction cascade (Gola et al., 2005). The reaction rate constants of $O(^1D)$ with H_2 and H_2O at 298 K are known to be 1.1 $x10^{-10}$ and 2.2 $x10^{-10}$ cm^3 s^{-1}, respectively (Burkholder et al., 2015). At a relative humidity of 70% (corresponding to 16000 µmol mol^{-1} at 20°C), the reaction with H_2O is by far the main pathway to form OH, with the H_2 pathway contributing about 4 % to the OH yield. The OH degradation experiments were also carried out with intermittent time intervals of photolysis and sampling. Ozone was added to the chamber for 2 – 20 min. After photolysis of O_3, the samples for subsequent carbon isotope analysis were sampled from the chamber and the photolysis cycle was started again. Experiments 1 to 3 were carried out with a Philips TUV lamp (55 W) and a mean O_3 mixing ratio of 620 nmol mol^{-1}. Under these conditions, the O_3 lifetime against photolysis was about 11 min. Hence, one can estimate a photolysis rate of $J(O_3)$ in the range of 1.5 x 10^{-3} s^{-1} for the first three experiments with CH_3Cl and a mean OH concentration of 2.9 x 10^9 molecules cm^{-3}.

For the experiments in the presence of CH_4, 4 Philips TUV lamps were installed around the chamber, which increased the $J(O_3)$ value. This is represented by the reduced lifetime of about 4 min for O_3 when the lamps were on and no O_3 was injected. From

the dilution corrected CH_4 loss rates, we calculated mean OH concentrations between 1.6×10^{10} and 2.0×10^{10} molecules cm^{-3} for these experiments.

Fig. S2 shows the degradation of CH_3Cl under these conditions as a typical example. In the absence of water vapor (exp. 3), the dilution-corrected CH_3Cl mixing ratios decreased by less than 3 % over 10h (fig. S3). This loss can be attributed to the reaction with OH originating from the reaction of H_2 with $O(^1D)$. In any case, this experiment provides an upper limit of 3% for contributions from other possible reactions and loss processes to the observed loss of CH_3Cl

The CH_4 and CO_2 mixing ratios as well as the dilution corrected CH_4 mixing from CH_4 control experiment are shown in fig. S4. The measured mixing ratios were corrected for the respective blanks of the zero air that were <0.01 µmol mol^{-1} for methane and 8.2±0.2 µmol mol^{-1} for CO_2. The CH_4 blank experiment was carried out with a dilution flow of 4 L min^{-1}. The slopes for CH_4 and CO_2 were -0.00118 and -0.00117min^{-1}, respectively. During this blank experiment, the dilution-corrected CH_4 mixing ratio changed by less than 0.2%. We can thus safely rule out any unaccounted loss of CH_4.

The extent of reaction from the CH_4 + OH isotope fractionation experiment CH_4 is displayed in Figure S5. The upper panel shows the extent of reaction, and the lower panel shows the corresponding O_3 mixing ratios. For this experiment, the dilution flow was reduced initially to 0.6 L min^{-1}. During this experiment, it was necessary to stepwise increase the dilution flow for maintaining an overpressure of 0.5 hPa inside the chamber. This resulted in a non-exponential loss due to dilution as shown in the CO_2 mixing ratios. The stepwise decrease in the CH_4 mixing ratios reflects the intermittent phases of ozone photolysis and sampling.

Potential effects of seasonal variations in the isotopic composition of the emissions on the tropospheric $\delta^{13}C(CH_3Cl)$

Here, we discuss in more detail how and to what extent uncertainties and potential seasonal variations in the isotopic source signals might affect the seasonality in the tropospheric $\delta^{13}C(CH_3Cl)$. We in particular analyzed, to what extent variations in the

isotopic source signal can mask the OH-loss driven seasonal signal in the tropospheric $\delta^{13}C(CH_3Cl)$

We modelled the effect of seasonal and random variations of up to ±10 ‰ in the combined source signature on the tropospheric $\delta^{13}C(CH_3Cl)$. The seasonal variations in the emissions are shown in figure 2 of the manuscript and the isotopic source signatures used here are displayed in table S1. Plant emissions from higher plants and the unknown sources were combined to one source with an isotopic source signature ranging from -110 ‰ , required to balance an ε value of -59 ‰ for the tropospheric sink, to -62 ‰ required to balance an ε value of -11.2 ‰, representing our best scenario with a tropical rainforest source of only 670 Gg a^{-1} and unknown sources of 1530 Gg a^{-1} having a $\delta^{13}C$ of -45 ‰. The isotopic source signatures were randomly on the 1σ level as stated in table 4 in the main manuscript using a Gaussian probability density function. 100 seasonal cycles were modeled with i: no fractionation assigned to the sinks showing the imprint of the combined source signature on the tropospheric $\delta^{13}C(CH_3Cl)$, ii: an ε value of -11.2 ‰ for the tropospheric loss and an ε value a KIE of -59‰ for the tropospheric loss.

As an example the results from a 10 year model run with fluctuations in the source signature between ± 5‰ and ±10 ‰ are shown in figure S5. The seasonal varying contributions mainly from biomass burning and “tropical rainforests / unknown” induce a seasonal cycle in the combined source signature with highest values occurring in March and the lowest values occurring in August. The amplitude of this cycle depends on the isotopic source signature assigned to “higher plants / unknown” and ranges from 12 ‰ for a source signature of -110 ‰ to 2.4 ‰ for a source signature of -62 ‰. In our model simulation this cycle is superimposed by the random variations in the source signatures (upper panel of figure S6). As already noted by Tans (1997) the large tropospheric background strongly attenuates temporal variations. In our model experiments seasonal variations in the source signature were attenuated in the troposphere by almost 80 % (panel 2 in figure S6).

Seasonal variations in the isotopic source signature between ± 5 ‰ and ±10 ‰ have a clear imprint on the tropospheric $\delta^{13}C(CH_3Cl)$ signal, when applying an ε value of -11.2 ‰ to the OH sink (panel 3, fig. S6). However these variations in the source signal are largely obscured, when applying an ε value of -59 ‰ to the OH sink (panel 4, fig. S6).

Depending on the phase displacement, any seasonal variation in the source signal can either amplify or attenuate the OH driven seasonal cycle in tropospheric $\delta^{13}C(CH_3Cl)$. The isotopic effect of the OH sink results in an inverse co-variation of the tropospheric $\delta^{13}C(CH_3Cl)$ with CH_3Cl mixing ratios. An amplification of this seasonal cycle arises when the most enriched source signatures coincide with the peak in OH loss and vice versa a coincidence of the most depleted source signatures with the peak OH loss will attenuate the OH driven seasonal cycle.

An ε value of -59 ‰ assigned to the OH sink results in a seasonal amplitude of 9 ‰ in the tropospheric $\delta^{13}C(CH_3Cl)$. Masking such a large isotope effect for the losses would require variations by about 50 ‰ in northern hemispheric emissions and seasonal variations of about 27 ‰ in the southern hemispheric emissions being inversely correlated to the OH loss in each hemisphere as depicted in figure S7 for the northern hemisphere.

From our simulations, we conclude that seasonal variations in the isotopic source signature of up to ±10 ‰ (being in the range of reported uncertainties) can obscure the OH-loss driven seasonal cycle in the tropospheric $\delta^{13}C(CH_3Cl)$, when applying an ε value of -11.2 ‰ to the OH sink but have a minor effect on the seasonal signal when applying an ε value of -59 ‰ to the OH sink. With respect to the reported source signatures and the interhemispheric distribution of the sources, any scenario where the seasonal variability of the strength and isotope ratios of CH_3Cl emissions nearly exactly balances the otherwise expected high seasonal variability of the carbon isotope ratio of CH_3Cl is highly unlikely.

References

Behnke, W., Holländer, W., Koch, W., Nolting, F., and Zetzsch, C.: A smog chamber for studies of the photochemical degradation of chemicals in the presence of aerosols, Atmos. Environ., 22, 1113–1120, 1988.

Bleicher S, Buxmann, J.-C., Sander, R., Riedel, T.P., Thornton, J.A., Platt, U, Zetzsch, C.: The influence of nitrogen oxides on the activation of bromide and chloride in salt aerosol, Atmos. Chem. Phys. Discuss., 14, 10135–10166, 2014.

Cantrell, C. A., Shetter, R. E., McDaniel, A. H., Calvert, J. G., Davidson, J. A., Lowe, D. C., Tyler, S. C., Cicerone, R. J., and Greenberg, J. P.: Carbon kinetic isotope effect in the oxidation of methane by the hydroxyl radical, Journal of Geophysical Research: Atmospheres, 95, 22455-22462, doi:10.1029/ JD095iD13p22455, 1990.

DeMore, W. B.: Rate constant ratio for the reaction of OH with CH_3D and CH_4, J. Phys. Chem., 97, 8564–8566, 1993.

Gola, A. A., D'Anna, B., Feilberg, K. L., Sellevåg, S. R., Bache-Andreassen, L., and Nielsen, C. J.: Kinetic isotope effects in the gas phase reactions of OH and Cl with CH_3Cl, CD_3Cl, and (CH_3Cl)-C-13, Atmos. Chem. Phys., 5, 2395-2402, 2005.

Keppler, F., Bahlmann, E., Greule, M., Schöler, H. F., Wittmer, J., and Zetzsch, C.: Mass spectrometric measurement of hydrogen isotope fractionation for the reactions of chloromethane with OH and Cl, Atmos. Chem. Phys., 18, 6625-6635, 10.5194/acp-18-6625-2018, 2018.

Madronich, S. and Flocke, S.: The role of solar radiation in atmospheric chemistry, in: The Handbook of Enviromental Chemistry, vol. 2, Part I: Environmental Photochemistry, edited by Boule, P., Springer, Berlin, 1–26, 1999.

Palm, W.-U., Elend, M., Krüger, H.-U., Zetzsch, C, OH radical reactivity of airborne Terbuthylazine adsorbed on inert aerosol, Environ. Sci. Technol., 31, 3389–3396, DOI: 10.1021/es970003k, 1997

Tans, P. P.: A note on isotopic ratios and the global atmospheric methane budget, Global Biogeochemical Cycles, 11, 77-81, doi:10.1029/96GB03940, 1997.

Supplementary Figures

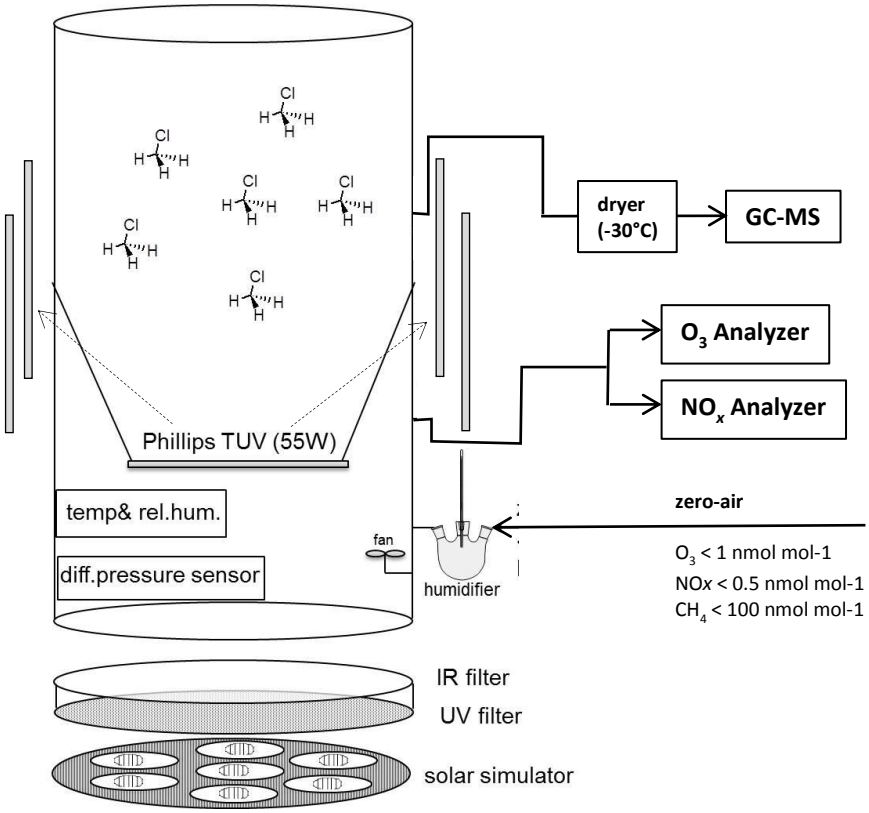

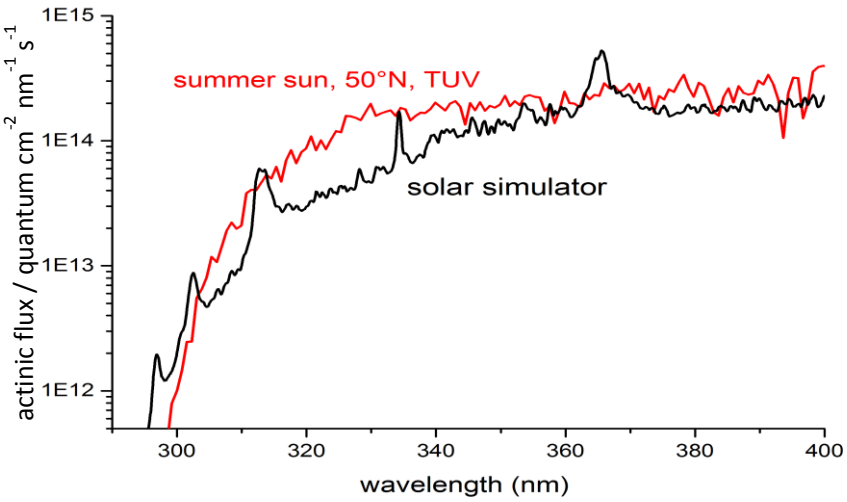

Figure S1: The upper panel (figure adopted from Keppler et al., 2018) shows the setup of the smog chamber used for the CH_3Cl degradation experiments, and the lower panel (Bleicher et al., 2014) shows the actinic flux of the solar simulator in comparison with a solar spectrum from the TUV model (Madronich and Flocke, 1989). The solar simulator (Behnke et al., 1988) was used for the photolytic production of atomic Cl, and one or four TUV lamps (Philips) for the photochemical production of OH by photolysis of O_3 at 253.7 nm.

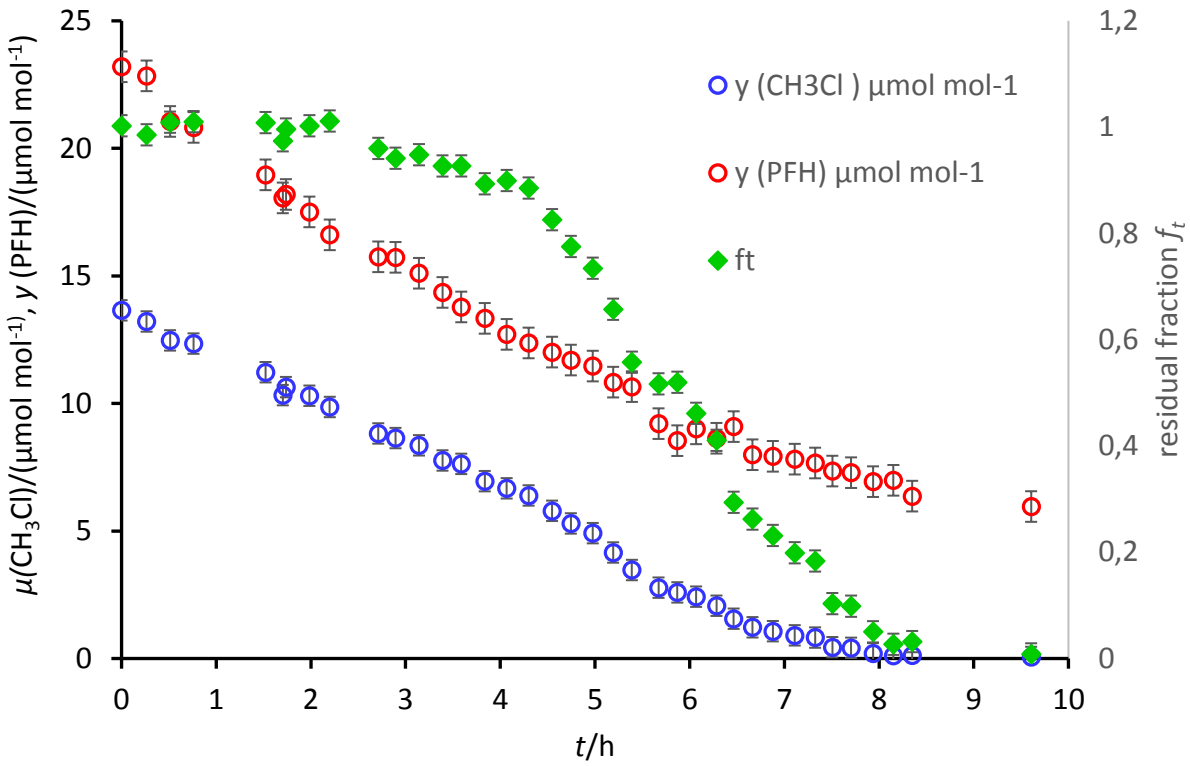

Figure S2: Extent of the CH_3Cl + OH reaction in experiment 3. The blue and red circles show the changes in the CH_3Cl and PFH abundance over time. The green diamonds show the residual fraction of CH_3Cl calculated from the ratio of CH_3Cl and PFH mixing ratios. The ozone photolysis was started after 2h. During this lag phase, the reproducibility for the determination of the residual fraction was 1.4 %.

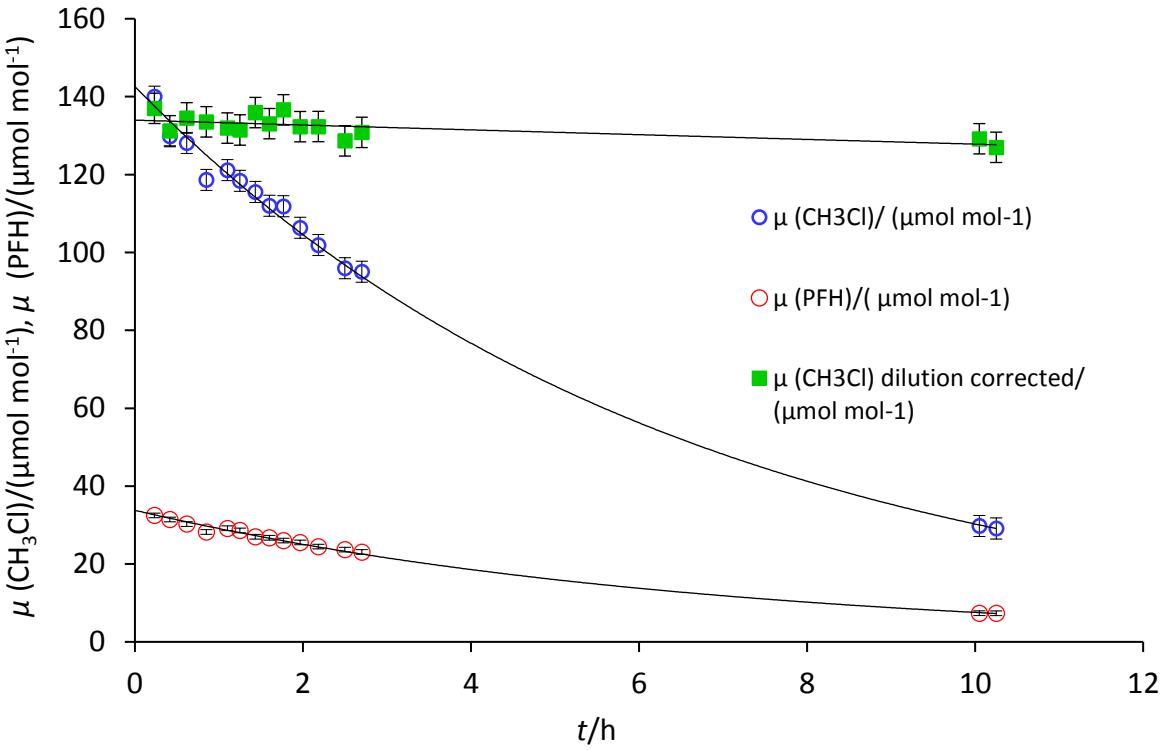

Figure S3: Extent of the CH_3Cl + OH reaction in the absence of water vapor. Ozone photolysis was started after 1 h. The blue and red circles show the changes in the CH_3Cl and PFH abundance over time. Initial mixing ratios were 133.5 µmol mol^{-1} for CH_3Cl and 25 µmol mol^{-1} for PFH. The dilution corrected mixing ratios of CH_3Cl shown in green decreased by less than 3% over ten hours ([CH_3Cl] = 133.5 x $e^{(-0.0042*t)}$, R^2 0.43) due to the insufficient OH generation in the absence of H_2O. The $\delta^{13}C$ values of CH_3Cl (not shown) were -46.8 ‰ at the beginning and -46.1 ‰ after 10h.

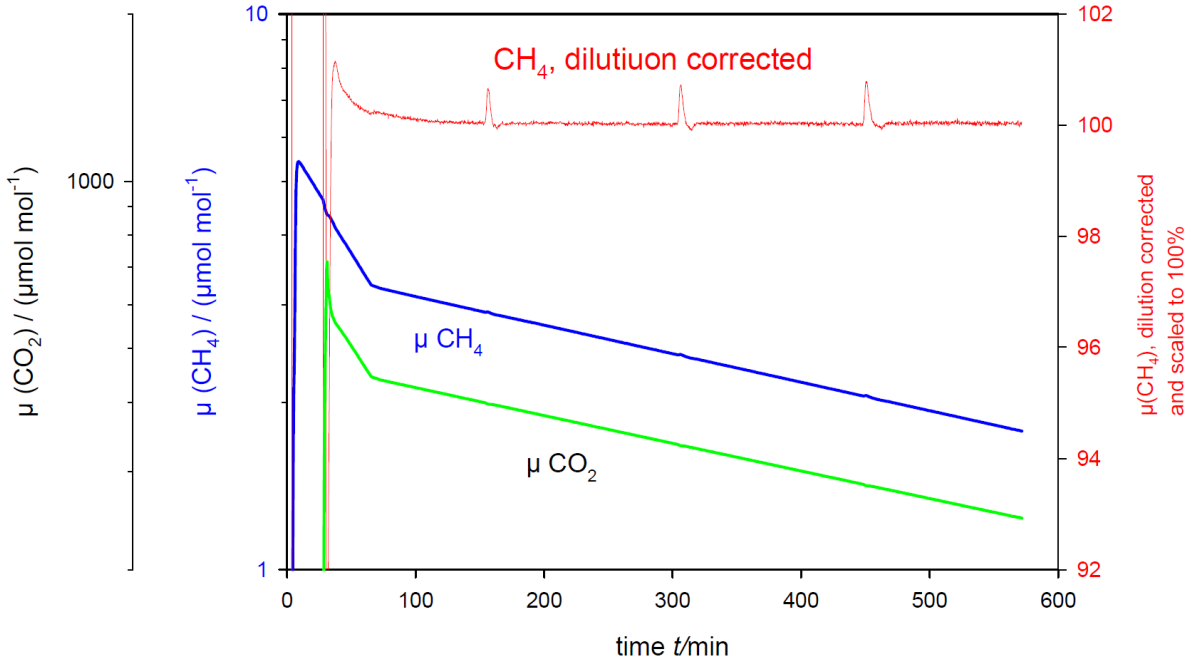

Figure S4 (data are from the supplement of Keppler et al., 2018): CH_4 blank experiment, illustrating mixing and exponential dilution, employing CO_2 as inert tracer. The blue and green lines show the measured CH_4 and CO_2 mixing ratios, respectively. The red line shows the dilution-corrected CH_4 mixing ratios using CO_2 as inert tracer and subtracting a background of 0.04 μmol mol^{-1} from CH_4.

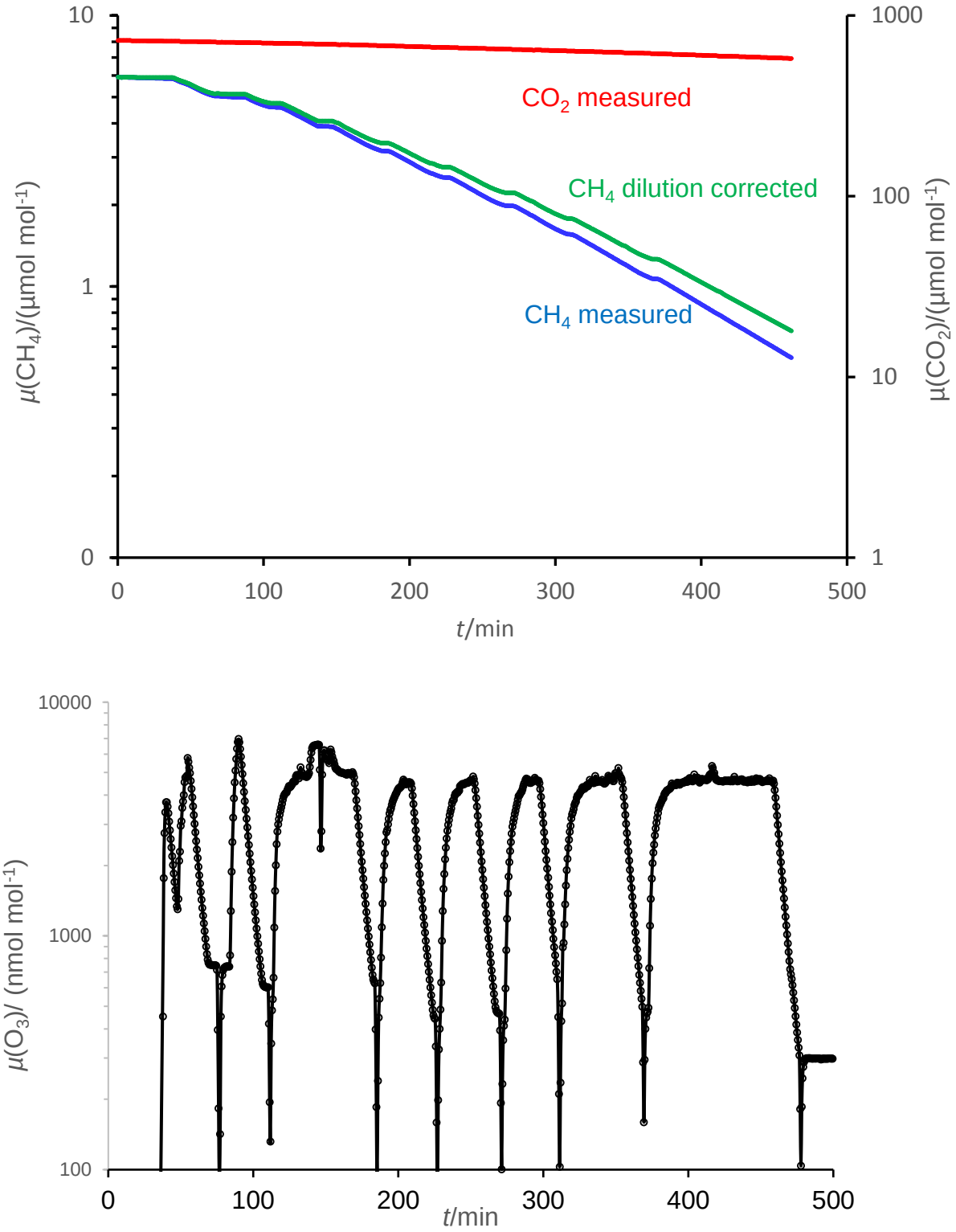

Figure S5 (data from the supplement of Keppler et al., 2018): Upper panel: CH_4+OH degradation experiment for stable carbon isotope measurements. The measured CH_4 mixing ratios (blue line) were corrected (green line) for dilution using CO_2 (red line) as an inert tracer. We noted a small spectral interference (<0.1%) in the CO_2 signal arising from ozone. The lower row panel shows the corresponding steady state mixing ratios of ozone. Ozone and UV-light were switched off from time to time to take the canister samples.

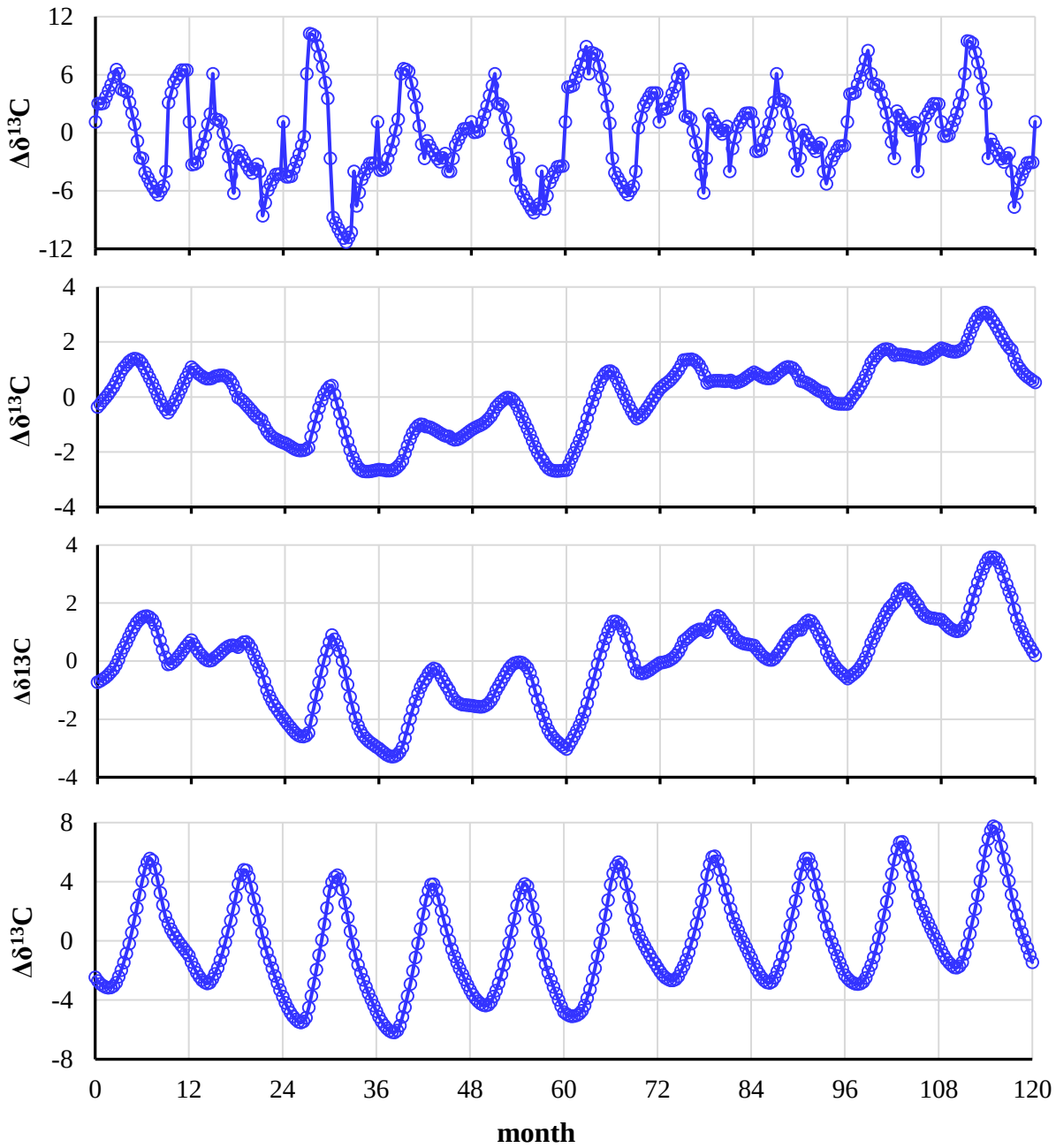

Figure S6: Variations in the isotopic composition of the combined CH_3Cl sources and of tropospheric CH_3Cl. Results from a ten-year simulation. The uppermost panel shows the combined isotopic composition of all sources with seasonal random variations of up to ±10 ‰ in the $\delta^{13}C$ of the combined sources. The second panel shows the resulting fluctuations in the isotopic composition of tropospheric CH_3Cl, with no isotopic fractionation assigned to the CH_3Cl sinks. The northern hemispheric background attenuates the variation in the isotopic source signature by about 80% resulting in seasonal variations of the northern hemispheric $\delta^{13}C$ between ±0.5 ‰ ±2 ‰. The third panel shows the seasonal fluctuations in the $\delta^{13}C$ of northern hemispheric CH_3Cl using an isotope effect of -11.2 ‰ for the OH sink and finally the fourth panel shows the respective seasonal variations for an isotope effect of -59 ‰ as suggested by Gola et al. (2005).

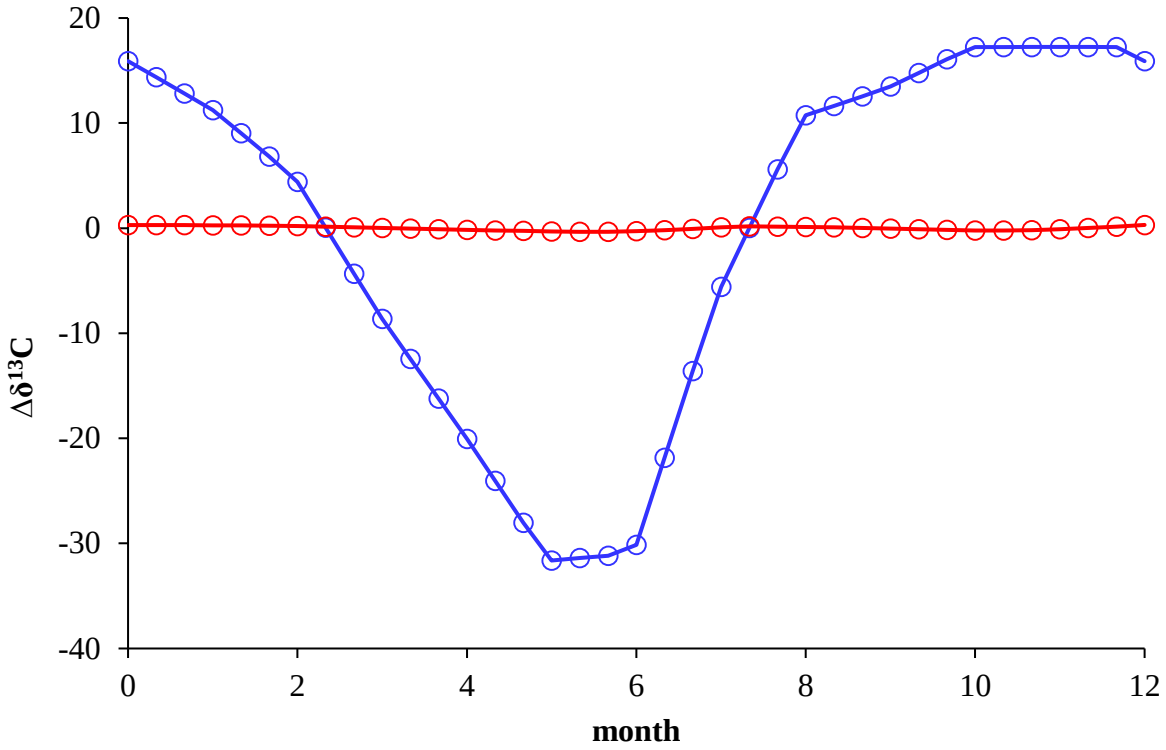

Figure S7: Seasonal variations in the combined isotopic source signature (blue circles) in the northern hemisphere required to balance the seasonal variations in the tropospheric $\delta^{13}C(CH_3Cl)$ (red circles(induced by an isotope effect of -59 ‰ for the OH sink as suggested by Gola et al. (2005).